Journal Pre-proofs

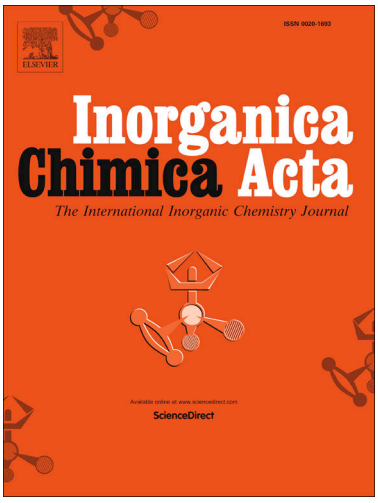

Research paper

Platinum and Palladium Complexes of Tridentate -C^N^N (Phen-ide)-pyridine-thiazol Ligands – A case study involving spectroelectrochemistry, photoluminescence spectroscopy and TD-DFT calculations

Maren Krause, René von der Stück, Dana Brünink, Stefan Buss, Nikos L. Doltsinis, Cristian A. Strassert, Axel Klein

PII: S0020-1693(20)31293-7
DOI: https://doi.org/10.1016/j.ica.2020.120093
Reference: ICA 120093

To appear in: *Inorganica Chimica Acta*

Received Date: 30 July 2020
Revised Date: 14 October 2020
Accepted Date: 17 October 2020

Please cite this article as: M. Krause, R. von der Stück, D. Brünink, S. Buss, N.L. Doltsinis, C.A. Strassert, A. Klein, Platinum and Palladium Complexes of Tridentate -C^N^N (Phen-ide)-pyridine-thiazol Ligands – A case study involving spectroelectrochemistry, photoluminescence spectroscopy and TD-DFT calculations, *Inorganica Chimica Acta* (2020), doi: https://doi.org/10.1016/j.ica.2020.120093

Platinum and Palladium Complexes of Tridentate ⁻C^N^N (Phen-ide)-pyridine-thiazol Ligands – A case study involving spectroelectrochemistry, photoluminescence spectroscopy and TD-DFT calculations

Maren Krause,[a] René von der Stück,[a] Dana Brünink,[b] Stefan Buss,[c] Nikos L. Doltsinis,[b,*] Cristian A. Strassert,[c,*] Axel Klein[a,*]

[a] Universität zu Köln, Department für Chemie, Institut für Anorganische Chemie, Greinstraße 6, D-50939 Köln, Germany
[b] Westfälische Wilhelms-Universität Münster, Institut für Festkörpertheorie and Center for Multiscale Theory and Computation, Wilhelm-Klemm-Straße 10, 48149 Münster, Germany
[c] Westfälische Wilhelms-Universität Münster, Institut für Anorganische und Analytische Chemie, CiMIC, CeNTech, SoN, Heisenbergstraße 11, D-48149 Münster, Germany

* to whom the correspondence should be addressed: e-mail: axel.klein@uni-koeln.de

Dedicated to Prof. Dr. Luisa De Cola on the occasion of her 60th birthday

Received *[Inorg. Chim. Acta] - VSI Photofunctional complexes*

Abstract:
Four Pd(II) and Pt(II) complexes [M(C^N^N)Cl] (HC^N^N = 2-(6-phenylpyridin-2-yl)thiazoles) were synthesised, analysed and characterised using ^{1}H NMR and MS in solution, as well as single crystal XRD in the solid. Cyclic voltammetry of the square planar complexes showed reversible or partially reversible reductions and irreversible oxidations. DFT calculations allowed assigning them to essentially metal-centred oxidations and ligand-centred reductions. Absorption spectra of the complexes show intense absorption bands into π-π* states in the UV to visible spectral range and long-wavelength bands which were assigned to transitions into mixed metal-to-ligand charge transfer (MLCT)/π-π* states, based on TD-DFT calculations. Comparison of Pt and Pd derivatives showed that the energy of the (MLCT)/π-π* bands are increased for Pd over Pt. This was also observed for the phosphorescence at 77 K and is attributed to the higher oxidation potential for Pd and supported by spectroelectrochemical measurements. The photoluminescence quantum yield (Φ_L) drops drastically from Pt to Pd at room temperature, where only the two Pt(II) complexes are luminescent showing a broad unstructured phosphorescence from a ^{3}MLCT state. At 77 K, the phosphorescence is blue-shifted and shows a clear vibrational progression, which is related to an enhanced ligand-centred character related to the lack of solvent stabilisation in the frozen matrix that otherwise increases the MLCT contribution. The Pd(II) complexes are not emissive at 298 K but luminesce at 77 K. This is due to metal-centred dissociative d-d* states that facilitate radiationless deactivation, which cannot be thermally populated at low temperatures. Thus, similar Φ_L are observed in frozen glassy matrices for both metals. TD-DFT calculations provided insight into the excited states and showed that the substitution pattern does not affect the emission, due to the lack of participation of the phenyl unit in the orbitals that are relevant for the description of the emissive state.

Keywords:
Platinum; Palladium; cyclometalating CNN ligands; electrochemistry, UV-vis absorption, photoluminescence

1. Introduction

The last two decades saw a tremendous development in the design and synthesis of cyclometalated Pt(II) and Pd(II) complexes for their use as triplet emitting materials.[1-22] The combination of the d^8 configured metal ions and π accepting ligands (low lying π* orbitals) allows to generate and tune very long-lived metal-to-ligand (MLCT) excited states.[1-27] Heteroaromatic structures have turned out to be very useful allowing the fine-tuning of various mixed MLCT / π–π* (IL) excited states.[1-27] Furthermore, rigidity of both the organic ligand and the square planar coordination around the metal are very important for efficient triplet emission since this helps avoiding effective radiationless decay.[7,10,16,18,19,21,22,25-30] Cyclometalated heteroaromatic ligands provide rigidity, a strong ligand field and suitable intraligand (IL) excited states and are thus frequently used.[1-30] Combined experimental / theoretical studies have related structural features with photoluminescence (PL) properties.[13,14,19-31] While structural (substitution) effects on the emission energy are today well understood through DFT modelling and emission energies can be almost deliberately tuned,[10,12,21,22,24,26,27,30] the PL efficiency, expressed as PL quantum yield (Φ_L) are less predictable.[10,21,22,27,28] This is due to the complex composition and dynamic behaviour of the excited states of transition metal complexes.[21,22,32]

Out of all the parameters crucial for the ligand-field splitting, the position in the periodic table is the most important one, but comparative studies with 4d and 5d metals from the same group are scarce.[4,6,11,15,32-47] In the last few years, we and others have devoted some work to this challenge and have managed to isolate and study isoleptic complexes of the group 10 metals Pt and Pd in their oxidation state +II.[33,35,37,39-47]

Herein, we report a study using the two metals and two different cyclometalating C^N^N ligands based on 2-(6-phenylpyridin-2-yl)thiazoles (Scheme 1). They represent the variation of the central pyridine to phenylpyridine and 3,5-(bis-*t*Bu)phenylpyridine which had turned out to be beneficial for the ability of such cyclometalated complexes for efficient triplet emission.[8,10,18,28-30] We studied the electrochemical and photophysical properties of the isoleptic Pd and Pt complexes in comparison. Important insight into the excited states properties and dynamics came from TD-DFT calculations.

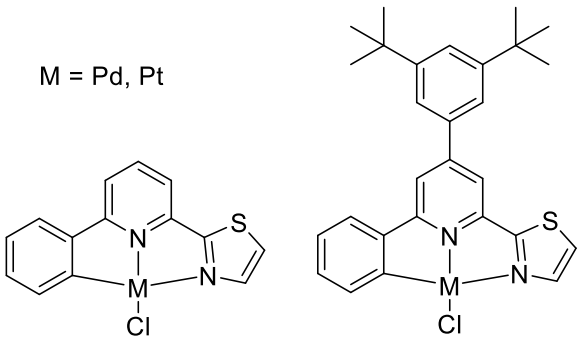

Scheme 1. Schematic representation of the [M(C^N^N)Cl] complexes.

2. Experimental

2.1 General information

Commercially available reagents from Merck, abcr, Apollo or Alfa Aesar were used without further purification. Acetone was dried over molecular sieves and distilled. THF for electrochemical experiments was dried over Na/K alloy and distilled. All reactions and measurements involving metal complexes were conducted under argon, using standard Schlenk techniques. The protoligands (ligands prior to deprotonation) and the complexes are air-stable solids.

2.2 Syntheses

2.2.1 Syntheses of ligand precursors and protoligands

The synthesis and detailed characterisation of the ligand precursors and the protoligands is provided in the Supplementary Material.

2.2.2 Synthesis of the complexes

Syntheses of the Pd complexes [Pd(C^N^N)Cl] - General description.

1 eq. of the HC^N^N protoligand was dissolved in MeCN and 1 eq. $K_2[PdCl_4]$ was added. The resulting off-white precipitate dissolved within a few seconds. The now brownish solution was heated to 90 °C. After the formation of a bright yellow precipitate the mixture was stirred at 90 °C for another 30 min. After cooling to ambient temperature, the solid was filtered off and washed with H_2O and MeCN. The yellow product was dried under reduced pressure for at least 3 h.

6-(phenyl-2-ide)-2-thiazolylpyridine-chlorido-palladium(II) [Pd(ph(py)tz)Cl]. From 238.3 mg (1 mmol) 6-phenyl-2-thiazolylpyridine, 326.4 mg (1 mmol) K_2PdCl_4, 25 mL H_2O + 25 mL MeCN. Yield: 346.6 mg (0.91 mmol, 91%) yellow solid. Anal. Calc. for $C_{14}H_9ClN_2PdS$ (379.17) C: 44.35, H 2.39, N: 7.39, S: 8.46. Found C: 44.38, H: 2.35,

N: 7.34, S 8.39%. ^{1}H NMR: (600 MHz, DMSO-d_6) δ = 8.21 (d, 1H, *J* = 3.2 Hz), 8.07 (t, 1H, *J* = 7.9 Hz), 8.01-7.89 (m, 2H), 7.84 (d, 1H, *J* = 3.2 Hz), 7.58 (dd, 1H, *J* = 7.2 Hz), 7.48 (dd, 1H, *J* = 7.2 Hz), 7.15-7.02 (m, 2H) ppm. ^{13}C NMR: (151 MHz, DMSO-d_6) δ = 166.85 (q), 164.00 (q), 153.41 (q), 149.42 (q), 147.69 (q), 142.04, 141.22, 136.38, 130.23, 126.42, 125.46, 125.35, 120.35, 120.22 ppm. EI-MS(+) (70 eV) m/z = 381 $[M+H]^+$, 344 $[M-Cl+H]^+$.

6-(pheny-2-ide)-2-thiazolyl-4-(3,5-(di-*t*-butylphen-1-yl)pyridine-chlorido-palladium(II) [Pd(ph(tbppy)tz)Cl]. From 426.6 mg (1 mmol) 6-phenyl-2-thiazolyl-4-(3,5-di-*t*-butylphen-1-yl)pyridine, 326.4 mg (1 mmol) K_2PdCl_4, 25 mL H_2O + 55 mL MeCN. Yield: 436.6 mg (0.77 mmol, 77%) yellow solid. Anal. Calc. for $C_{28}H_{29}ClN_2PdS$ (567.48) C: 59.26, H 5.15, N: 4.94, S: 5.65. Found C: 59.38, H: 5.25, N: 4.94, S 5.63%. ^{1}H NMR: (600 MHz, DMSO-d_6) δ = 8.21 (d, 1H, *J* = 3.2 Hz), 8.17 (d, 1H, *J* = 1.5 Hz), 8.09 (d, 1H, *J* = 1.5 Hz), 7.79 (dd, 2H, *J* = 7.0 Hz), 7.74 (d, 2H, *J* = 1.8 Hz), 7.59 (t, 1H, *J* = 1.7 Hz), 7.44 (dd, 1H, *J* = 7.6 Hz), 7.07 (td, 1H, *J* = 7.4 Hz), 6.99 (td, 1H, *J* = 7.4 Hz), 1.40 (s, 18H) ppm. ^{13}C NMR: (151 MHz, DMSO-d_6) δ = 166.9 (q), 164.0 (q), 153.5 (q), 153.4 (q), 151.8 (q), 149.6 (q), 147.8 (q), 141.8, 136.4 (q), 136.2, 130.0, 126.3, 125.9, 125.0, 124.3, 122.5, 118.5, 118.0, 40.3, 35.4, 31.7 ppm. EI-MS(+) (70 eV): m/z = 569 $[M+H]^+$, 532 $[M-Cl+H]^+$.

Synthesis of 6-(phenyl-2-ide)-2-thiazolylpyridine-chlorido-platinum(II) [Pt(ph(py)tz)Cl]. 119 mg (0.5 mmol) 6-phenyl-2-thiazolylpyridine (Hph(py)tz) was dissolved in 12.5 mL MeCN and added to a solution of 208 mg (0.5 mmol) $K_2[PtCl_4]$ in 12.5 mL H_2O. The reaction mixture was heated up to 90 °C and stirred for 24 h leading to an orange precipitate. After cooling to ambient temperature, the solid was filtered off and washed with H_2O and MeCN. The orange product was dried in vacuo. Yield: 148 mg (0.32 mmol, 63%). Anal. Calc. for $C_{14}H_9ClN_2PtS$ (467.83) C: 35.94, H 1.94, N: 5.99, S: 6.85. Found C: 35.95, H: 1.95, N: 6.00, S 6.86%. ^{1}H NMR (600 MHz, DMSO-d_6) δ = 8.37 (d, 1H, *J* = 3.2 Hz), 8.03 (t, 1H, *J* = 7.9 Hz), 7.98-7.96 (m, 2H), 7.86 (d, 1H, *J* = 7.9 Hz), 7.54 (dd, 1H, *J* = 0.8, 7.6 Hz), 7.42 (dd, 1H, *J* = 0.8, 7.5 Hz, J_{Pt-H} = 42.3 Hz), 7.11 (dt, 1H, *J* = 1.2, 7.4 Hz), 7.05 (t, 1H, *J* = 7.4 Hz) ppm. HR-ESI-MS(+): *m*/*z* = 460.01905 $[M-Cl+N_2]^+$ (calc. 431.010759), 431.01055 $[M-Cl]^+$ (calc. 460.019583).

Synthesis of 6-(pheny-2-ide)-2-thiazolyl-4-(3,5-di-*t*-butylphen-1-yl)pyridine-chlorido-platinum(II) [Pt(ph(tbppy)tz)Cl]. A mixture of 208 mg (0.5 mmol) $K_2[PtCl_4]$ and 256 mg (0.6 mmol) Hph(tbppy)tz were suspended in acetic acid (60 mL). The mixture was heated up to 110 °C and stirring was continued for 3 d. After cooling the reaction mixture, the precipitate was filtered off and washed with acetic acid, water and diethyl ether. The orange product was dried in vacuo. Yield: 247 mg (0.4 mmol, 80%). Anal. Calc. for $C_{28}H_{29}ClN_2PtS$ (656.15) C: 51.25, H 4.46, N: 4.25, S: 4.89. Found C: 51.28, H: 4.44, N: 4.25, S 4.88%. ^{1}H NMR (600 MHz, CD_2Cl_2) δ = 7.84 (d, 1H, *J* = 3.2 Hz), 7.71 (d, 1H, *J* = 3.2 Hz), 7.64 (t, 1H, *J* = 1.7 Hz), 7.57-7.56 (m, 3H, *J* = 1.7 Hz), 7.43-7.42 (m, 2H, *J* = 2.7 Hz, J_{Pt-H} = 45.3 Hz), 7.32 (dd, 1H, *J* = 1.4, 7.4 Hz), 7.05-6.99 (m, 2H, *J* = 3.2 Hz), 1.45 (s, 18H) ppm. EI-MS(+) (70 eV) m/z = 656 $[M]^+$, 426 $[ph(tbppy)tz]^+$.

2.3 Instrumentation

^{1}H and ^{13}C NMR spectra were recorded on a Bruker Avance II 300 MHz (^{1}H: 300.13 MHz, ^{13}C: 75.47 MHz) - double resonance (BBFO) 5 mm observe probehead with z-gradient coil, Bruker Avance 400 MHz (^{1}H: 400.13 MHz, ^{13}C: 100.61 MHz) using a triple resonance ^{1}H, BB inverse probe head or Bruker Avance II 600 MHz spectrometer (^{1}H: 600.13 MHz, ^{13}C: 150.93 MHz) with a triple resonance (TBI) 5 mm inverse probehead with z-gradient coil using a triple resonance. The unambiguous assignment of the ^{1}H resonances was obtained from ^{1}H NOESY and ^{1}H COSY experiments. All 2D NMR experiments were performed using standard pulse sequences from the Bruker pulse program library. Chemical shifts are relative to TMS respectively. UV-vis absorption spectra were recorded with Varian Cary 05E or Cary 50 scan spectrophotometers. PicoQuant Fluo-Time 300 spectrometer was used for lifetime measurements. Lifetime analysis was performed using the commercial FluoFit software. The quality of the fit was assessed by minimising the reduced chi-squared function. Luminescence quantum yields were determined with a Hamamatsu Photonics absolute PL quantum yield measurement system (C9920–02), equipped with a L9799-01 CW Xenon light source, monochromator, photonic multichannel analyser and integrating sphere (uncertainty of roughly ± 2 % for Φ_L is estimated). All solvents were of spectroscopic grade. Elemental analyses were obtained using a HEKAtech CHNS EuroEA 3000 analyzer. EI-MS spectra were measured with a Finnigan MAT 95, and HR-ESI-MS using a THERMO Scientific LTQ Orbitrap XL. MS Simulations were performed using ISOPRO 3.0. IR spectra were measured in ATR mode using a Perkin Elmer 400 FT-IR spectrometer. Electrochemical measurements were carried out in 0.1 M nBu$_4$NPF$_6$/THF solution using a three-electrode configuration (glassy carbon working electrode, Pt counter electrode, Ag/AgCl reference electrode) and a Metrohm Autolab PGSTAT30 potentiostat and function generator or a SP-150 BioLogic potentiostat. The ferrocene/ferrocenium couple served as internal reference. UV-vis-spectroelectrochemical measurements (in 0.1 M nBu$_4$NPF$_6$/THF solution) were performed using an optically trans-parent thin-layer electrode (OTTLE) cell [48,49] at room temperature.

2.3 Single Crystal X-ray Diffractometric Analysis

XRD single crystal structure analysis for [Pd(ph(py)tz)Cl] ($P2_1/c$, No. 14) was performed using graphite-monochromated Mo-K$_\alpha$ radiation (λ = 7.1073 Å) with an IPDS II (STOE and Cie.) diffractometer. The structure was solved by direct methods using SIR2014 [50] and refinement was carried out with SHELXL 2016 [51] employing full-matrix least-squares methods on $F_0^2 \geq 2\sigma(F_0^2)$. The non-hydrogen atoms were refined with anisotropic displacement parameters without any constraints. The hydrogen atoms were included by using appropriate riding models, full data in the Supplementary Material or can be obtained free of charge at https://summary.ccdc.cam.ac.uk/structures or from the Cambridge Crystallographic Data Centre, 12 Union Road, Cambridge, CB2 1EZ UK (fax: +44-1223 336033 or e-mail: deposit@ccdc.cam.ac.uk), CCDC 2006642.

2.5 DFT calculations

The optimised geometries and the vibrational Franck–Condon spectra were determined with the quantum chemistry package Gaussian 09 Rev. D.01 [52] using the CAM-B3LYP functional [53] together with Grimme's D3 dispersion correction with Becke-Johnson damping.[54] The SDD basis set applies an effective core potential for the Pt and Pd atoms,[55] while the D95 basis set is used for H, C, N, and O atoms.[56]

To compute vibrational Franck–Condon spectra, the method of Barone et al.[57,58] with Kohn–Sham DFT-based geometry optimisations in the S0 and T1 states followed by frequency analysis calculations was used.

All energy corrections were done by adding zero-point vibrational energies and thermal free energy contributions. To calculate the overlap integrals for the vibronic spectra, the transitions are divided into classes Cn, where n is the number of the excited normal modes in the final electronic state. The number of quanta per mode was limited to 100 while the number of quanta for combinations of two modes was restricted to 65. The maximum number of computed integrals was set to 1.5×10^8. A maximum of 20 classes was calculated. The line spectrum was broadened with the aid of gaussian functions with a half-width at half-maximum of 400 cm^{-1}.

The solvent CH_2Cl_2 was taken into account by the polarisable continuum model (PCM) in an integral equation formalism framework [59] with atomic radii from the universal force field model (UFF).[60] To characterise the emissive T_1 state, the T_1 geometry was first optimised with Kohn–Sham DFT with multiplicity 3 followed by TD-DFT calculations of the T_1 state. TD-DFT calculations of the 40 lowest excited singlet states were performed at the optimised S_0 geometry with the PBE0 functional [61] and the SDD basis set to obtain the UV–vis absorption spectrum of the complexes [M(ph(py)tz)Cl] and [M(ph(tbppy)tz)Cl]. Finally, a Lorentzian broadening with a half-width at half-maximum (HWHM) of 10 nm was used for each transition.

3. Results and Discussion

3.1 Synthesis and General Characterisation

The protoligands (ligand precursors prior to cyclometalation) HC^N^N were assembled from corresponding Mannich bases or Chalcones using the versatile Kröhnke synthesis (details in the Supplementary Material). The Pt and Pd complexes were synthesised from the HC^N^N protoligands and $K_2[MCl_4]$ (M = Pt or Pd) and the complexes were obtained in 63 to 91% yield as yellow to orange microcrystalline powders. The materials were analysed and characterised through elemental analysis, ^{1}H NMR spectroscopy, and MS. Single crystal XRD of the complex **[Pd(ph(py)tz)Cl]** revealed the expected square planar geometry of these complexes and the binding through the N atom of the thiazol ligand moiety (Figure S8 and more details in the Supplementary data). The completely planar molecules stack in multiple ways in the crystal with π stacking interplanar distances of 3.89 and 3.98 Å, short Pd···arene contacts of 3.64 Å. The Pd atoms show a zig-zag pattern with Pd···Pd contacts of 4.7582(8) and 4.7561(8) Å (Figure S8)

3.2 Electrochemistry and DFT-calculated frontier orbitals of the complexes

On first view, all the cyclometalated complexes showed a first reversible one-electron reduction wave at around –1.7 V (Figure 1 and Figures S11-S14). The potentials are higher (less negative) for the Pt complexes (Table 1) compared with the Pd derivatives and slightly higher for the *t*Bu-phenyl complexes. They are usually followed by a second fully or partly reversible reduction wave at potentials around –2.45 V. These potentials are quite invariant. Similar behaviour was observed for the protoligands HC^N^N at potentials lying about 0.7 V lower than those of the complexes (Figure S2 and Table 1). We assume essentially ligand-centred reduction processes, in line with reports of similar complexes.[8,10,62-67] Thus, the deprotonation, metal coordination and planarisation of the ligand markedly shifts the reduction potentials by 0.7 V to 0.8 V. This is more pronounced for Pt(II) than for Pd(II). On the anodic side, irreversible oxidations are recorded in the range 0.54 V to 0.87 V (Table 1). Since the potentials for the Pt complexes lie somewhat lower than those of the Pd derivatives we can assume metal (M^{II}/M^{III}) based oxidation processes in line with previous reports.[8,10,62-67]

According to our DFT calculations, the LUMO is slightly more stable (by 0.06 eV) in the Pt complexes, while the HOMO is considerably less stable by 0.23 eV than in the Pd complexes (see Table S6, for plots see Figure S15) completely in line with the observed trend in the reduction potentials. This leads to the HOMO-LUMO gap in the Pt complexes being smaller by 0.23 eV compared to the Pd complexes. The effect of the ligand (i.e. py vs. tbppy), on the other hand, is found to be considerably smaller, the LUMO being lower by 0.01 eV and the HOMO by 0.02 eV with py. This is consistent with the small observed changes in the reduction potentials when changing from py to tbppy.

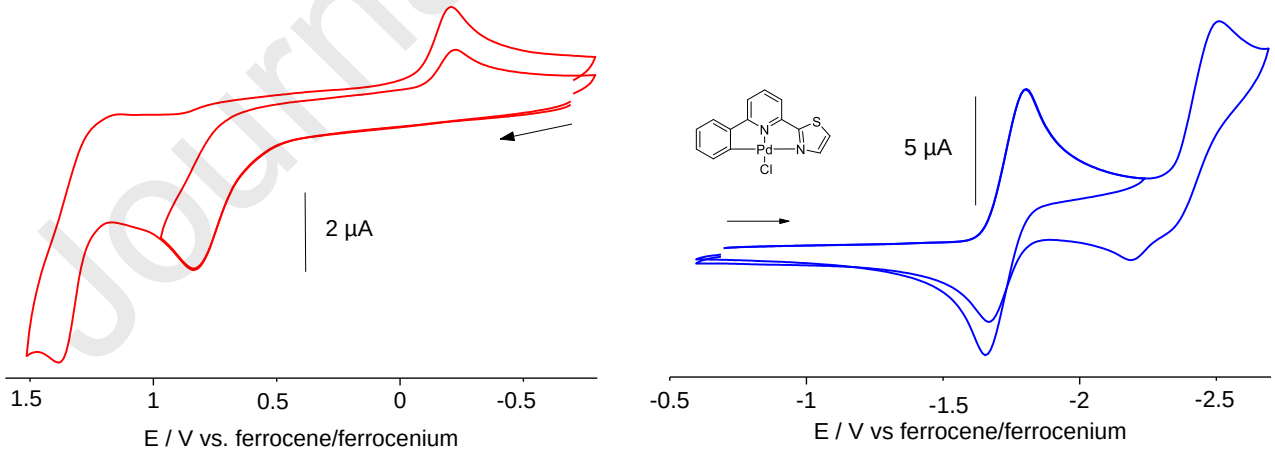

Figure 1. Cyclic voltammogramms of **[Pd(ph(py)tz)Cl]** in 0.1 M nBu$_4$NPF$_6$/solvent at 298 K and 0.1 V/s scan rate. Oxidations (left) in MeCN, reductions (right) in THF.

Table 1. Redox potentials of HC^N^N protoligands and [M(C^N^N)Cl] (M = Pd or Pt) complexes.[a]

	Ox2 E_{pa}	Ox1 E_{pa}	Red1 $E_{1/2}$	Red2 $E_{1/2}$	ΔE_{Red1}–E_{Ox1}
Hph(py)tz	-	-	–2.43	–3.32	-
Hph(tbppy)tz	-	-	–2.47	–3.37	-
[Pd(ph(py)tz)Cl]	1.38 [b]	0.84 [b]	–1.74	–2.44	2.58
[Pd(ph(tbppy)tz)Cl)]	1.10 [b]	0.87 [b]	–1.71	–2.45	2.58
[Pt(ph(py)tz)Cl]	> 1.3 [c]	0.64 [c]	–1.66	–2.39	2.30
[Pt(ph(tbppy)tz)Cl)]	1.14 [c]	0.66 [c]	–1.65 [c]	–2.35 [c]	2.31

[a] From cyclic voltammetry, electrochemical potentials in V (uncertainties ~5 mV), half-wave potentials $E_{1/2}$ for reversible redox waves and anodic peak potentials E_{pa} for irrevsible oxidation waves; measured in 0.1 M nBu$_4$NPF$_6$/THF at 298 K, scan rate 100 mV/s. [b] Measured in MeCN. [c] Measured in CH_2Cl_2.

The DFT calculated lowest unoccupied molecular orbitals (LUMO) of the complexes (Figure S15, compare also Figure 5) show contributions delocalised over the py-tz electron accepting part of the ligand and no contribution from the tBu$_2$-phenyl substitutent, which is in line with our assumptions for reductions. The calculated highest occupied molecular orbitals (HOMO) of the complexes obtain their highest contributions from the phenyl group and the metal, but also a small contribution from the central pyridyl moiety. The contribution of the metal atom to this orbital is similar for both Pt and Pd. The difference in oxidation potential for the two Pd/Pt pairs can be explained by the difference in HOMO energies (see Table S6). For the HOMO-1 similar contributions were found, now with a marked contribution of the chloride coligand. The HOMO-2 is clearly centred on the metal and chloride coligand.

3.3 UV-vis absorption / photoluminescence spectroscopy and TD-DFT calculations

The absorption spectra of the Pt and Pd complexes are dominated by intense absorption bands into π-π* states, peaking in the UV to visible range (Figure 2). When comparing the absorption maxima, the bands of the Pt complexes are slightly red-shifted compared with the Pd derivatives. Based on comparison with similar complexes,[8-10,15,23,31,32] we attribute this to a marked MLCT character of the corresponding excited states, which are energetically lowered for the less electronegative metal centre (Pt is easier to be oxidised than Pd). Similar intense bands were also seen in the HC^N^N protoligands (Figure S1) and their overall appearance of the vibrational progression depends strongly on the type of ligand.

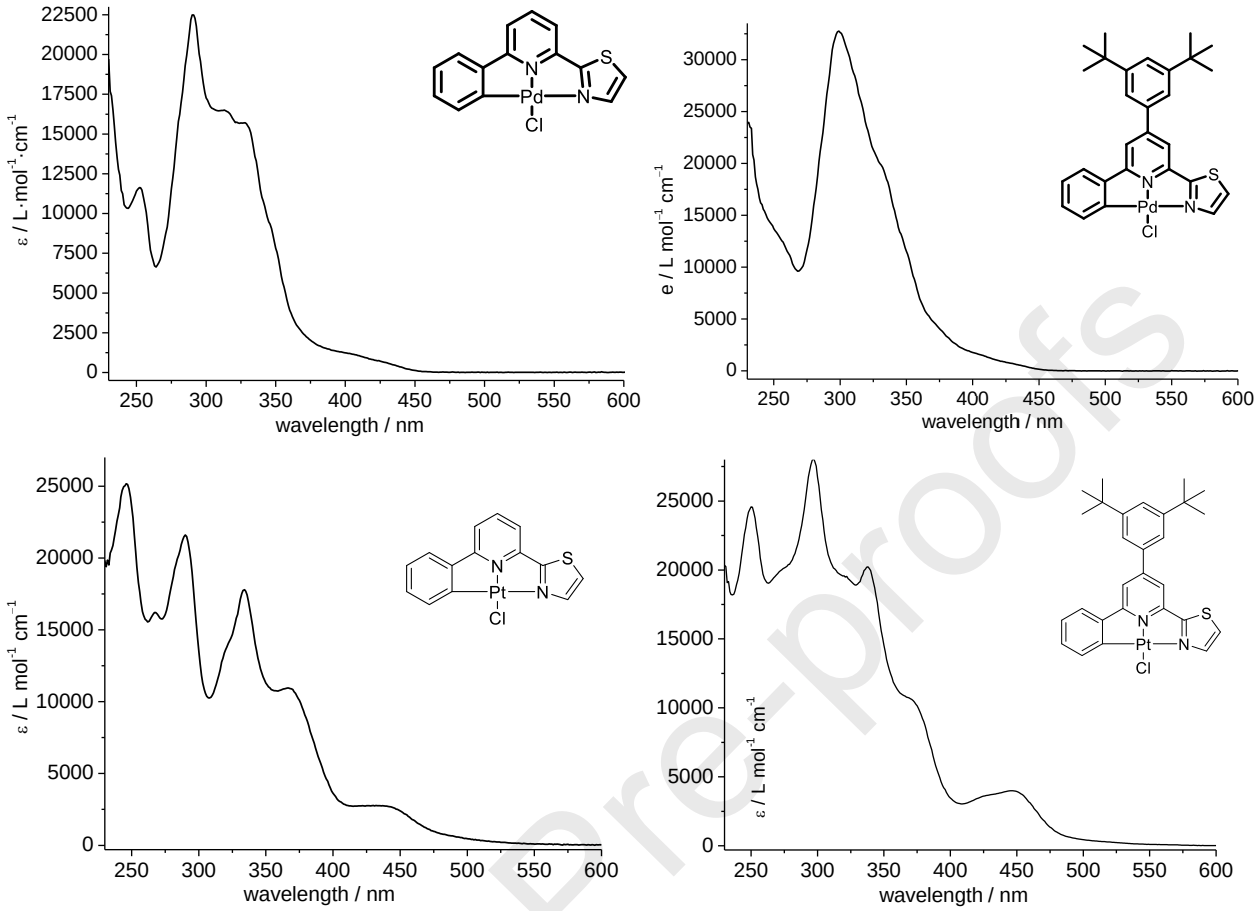

Figure 2. UV-vis absorption spectra (molar absorption coefficients as a function of wavelength) of the four complexes in fluid CH_2Cl_2 at RT.

The long-wavelength absorption bands of the complexes reveal significant differences between the Pt and Pd derivatives. While the spectra of the Pt complexes are characterised by broad bands peaking around 450 nm with molar absorption coefficients of around 3500 $M^{-1}{\cdot}cm^{-1}$, much weaker absorptions (shoulders) were observed for the Pd derivatives with markedly blue-shifted energies, when compared with the analogous Pt complexes (Table 2). For the other maxima, similar blue-shifts were observed when comparing the peaks at 400 (Pd) vs. 420 nm (Pt) and 340 (Pd) vs. 370 nm (Pt). This effect is consistent with the higher oxidation potentials observed in this report and in previous studies [33,35] for the more electronegative Pd compared with Pt and the assumed partial MLCT character of the excited states,[21,25,31,33,42,44] very probably with markedly different MLCT character when two metals are exchanged. This is consistent with the different contributions of the metal to the HOMO as outlined above. Higher MLCT character of the long-wavelenth band for the Pt complexes contrast probably with higher L(Phenyl)L(py-tz)CT character for Pd. The same blue-shifts were observed also for the quite similar complex pair [M(phbpy)Cl] (Hphbpy = 6-phenyl-2,2′-bipyidine) and further isoleptic pairs of Pd and Pt

complexes.[42,47,67-69] Interestingly, the absorption energies ot the phbpy complexes are very similar to the corresponding [M(ph(py)tz)Cl] derivatives, thus the thiazol group does not differ largely from a pyridyl unit.

Table 2. Selected photophysical data of [M(C^N^N)Cl] complexes.

Complex			**[Pt(ph(py)tz)Cl]**	**[Pt(ph(tbppy)tz)Cl]**	**[Pd(ph(py)tz)Cl]**	**[Pd(ph(tbppy)tz)Cl]**
λ_{abs} / nm (ε / 10^3 M^{-1} cm^{-1})[a]			366 (11.1), 421 (2.76), 436[b] (2.80)	376 (10.8), 424 (3.66), 446[b] (4.21)	344 (9.62), 401 (1.24), 423[b] (0.74)	346 (13.5), 402 (1.78), 427[b] (0.79)
Fluid solution (CH_2Cl_2, 298 K)	λ_{exc} / nm		294, 336, 370, 445	301, 340, 370, 446	n.d.	n.d.
	λ_{em} / nm		605, 640 sh	608	n.d.	n.d.
	τ / µs[e]	Air[c]	0.2452 ± 0.0018	0.275 ± 0.002	n.d.	n.d.
		Ar[d]	0.602 ± 0.018 [1.30 ± 0.16 (1); 0.594 ± 0.005 (99)]	0.714 ± 0.006	n.d.	n.d.
	Φ_L (± 0.02)	Air[c]	< 0.02	0.03	n.d.	n.d.
		Ar[d]	0.05	0.07	n.d.	n.d.
Frozen glassy matrix (CH_2Cl_2/MeOH 1:1, 77 K)	λ_{exc} / nm		294, 327, 360, 422	300, 333, 360, 429	290, 327, 380, 422	301, 325, 426
	λ_{em} / nm		557, 605, 660 (sh)	557, 603, 662 sh	520, 535, 558, 604, (672 sh)	517, 557, 604, (660 sh)
	τ / µs		3.17 ± 0.12 [3.65 ± 0.03 (44); 2.80 ± 0.03 (56)][f]	4.01 ± 0.13 [7.1 ± 0.3 (5); 3.84 ± 0.04 (95)][f]	95 ± 4 [105.9 ± 1.0 (74); 74 ± 3 (26)][g]	94 ± 3 [107 ± 1.0 (61); 75 ± 2.0 (39)][g]
	Φ_L (± 0.1)		0.18	0.22	0.13	0.19

[a] Measured in CH_2Cl_2. [b] Absorption maximum with the longest wavelength. [c] Aerated sample. [d] Deaerated sample (Ar-purged by bubbling for 20 min). [e] Photoluminescence decays measured detecting at 600 nm. [f] At 560 nm or [g] at 520 nm. For multiexponential decays, the amplitude-weighted average lifetimes are given as well as the different components in square brackets with relative amplitudes as percentages in parentheses.

Figure 3 shows the photoluminescence (PL) spectra of the complexes, their photophysical properties are summarised in Table 2 (the complete set of spectra and photoluminescence decay plots are shown in Figure S20 – S31). For the complex [**Pt(ph(py)tz)Cl**] at room temperature, the emission spectrum shows a single broad (unstructured) band with λ_{max} = 605 nm. This suggests, together with an excited state lifetimes (τ) of τ = 0.2452 μs, a clear overall MLCT character for the emissive state. The τ and Φ_L increase in the deaerated solutions, pointing to a quenching of the excited triplet state (^{3}MLCT) by $^3O_2$. At RT, the Pd(II) complexes are non-luminescent. At 77 K in frozen glassy matrices, the λ_{max} (557 nm) appeared strongly blue-shifted ($\Delta\lambda$ = 48 nm) if compared with their Pt(II) analogues and showed clear vibrational progressions (Figure 3; left). τ and Φ_L rise to τ = 3.17 μs and Φ_L = 0.18. Due to the lack of solvent stabilisation, the excited states possess less MLCT character and a clear metal-perturbed ligand-centred nature (^{3}MP-LC) as an admixture of LC character with minor MLCT contributions, which explains the structured vibrational progression and prolongued lifetimes.

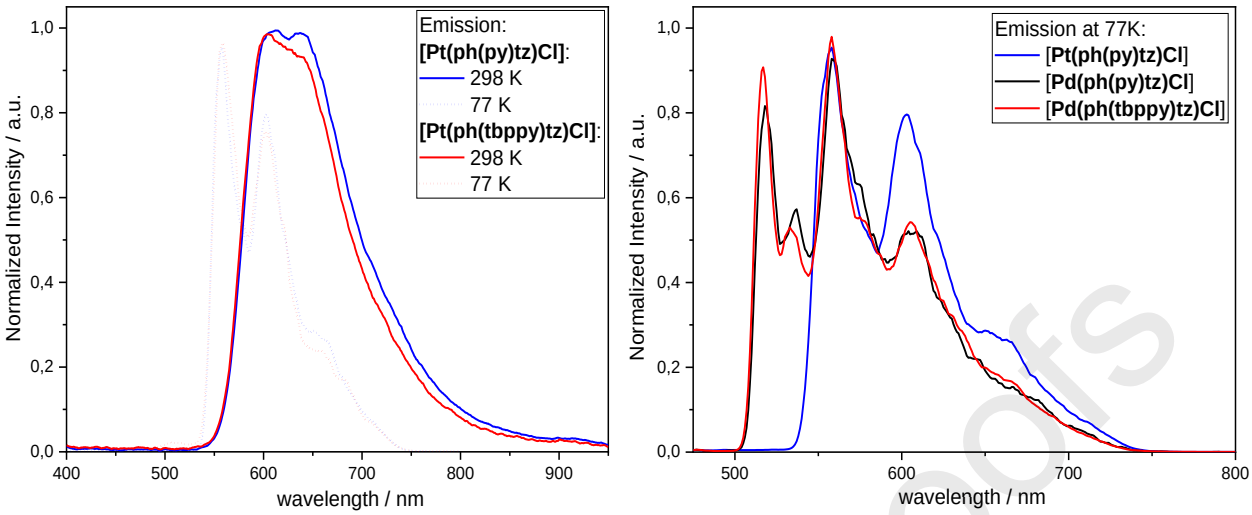

Figure 3. Left: Photoluminescence spectra (λ_{exc} = 350 nm) of **[Pt(ph(py)tz)Cl]** (blue) and **[Pt(ph(tbppy)tz)Cl]** (red) in fluid CH_2Cl_2 at 298 K (solid line) and in in a frozen glassy matrix (CH_2Cl_2/MeOH 1:1) at 77 K (dotted line). **Right:** Photoluminescence spectra (λ_{exc} = 350 nm) of **[Pt[ph(py)tz)Cl]** (blue), **[Pd(ph(py)tz)Cl]** (black) and **[Pd(ph(tbppy)tz)Cl]** (red) in a frozen glassy matrices (CH_2Cl_2/MeOH 1:1) at 77 K.

The change of the substitution pattern [**Pt(ph(tbppy)tz)Cl**] has no significant effect on the emission maxima as well as on the radiative and radiationless deactivation rates, as the lifetimes and quantum yields remain invariant within the experimental uncertainty, both at RT and at 77 K. In fact, the change upon sustitution is only marginal at 77 K, reaching τ = 4.01 μs and Φ_L = 0.22. Due to low-lying dissociative metal-centred d-d*-states related to a lower ligand field splitting, none of the Pd complexes shows detectable emission in fluid solutions at room temperature. On the other hand, at 77 K, the photoluminescence efficiency is comparable to the Pt complexes ($\Phi_{L[Pt(ph(tbppy)tz)Cl]}$ = 0.22 vs. $\Phi_{L[Pd(ph(tbppy)tz)Cl]}$ = 0.19). As in the case of the analogous Pt complexes at 77 K, the emission from the Pd complexes shows strong vibrational progressions (Figure 3; right). Due to the larger HOMO-LUMO gap of the Pd complexes, the emission appears blue-shifted ($\Delta\lambda \approx 30$ nm), if compared with the emission of the corresponding Pt complexes. The extremely long excited state lifetime for the Pd complexes ($\tau_{[Pd(ph(py)tz)Cl]}$ = 95.0 μs and $\tau_{[Pd(ph(tbppy)tz)Cl]}$ = 94.1 μs) can be attributed to the lower spin-orbit coupling of Pd compared with Pt, which affects the radiative and radiationless deactivation rate constants to a similar extent, thus prolonging the lifetimes while leaving the quantum yields unaffected.[31]

The different temperature-dependent photoluminescence behaviour of Pd and Pt complexes is in line with similar observations for related pairs of Pd and Pt complexes, especially for the very similar complexes [M(phbpy)Cl] (Hphbpy = 6-phenyl-2,2'-bipyidine) and derivatives.[42,47,67,68] In contrast to the absorption energies, the emission energies of the phbpy complexes are markedly blue-shifted compared to the ph(py)tz derivatives. E.g. [Pt(phbpy)Cl] shows a broad emission band with a maximum at 568 nm at 298 K in CH_2Cl_2 solution [67] compared with 602 nm for **[Pt(ph(py)tz)Cl]** and the high-energy maximum at 538 nm in glassy

frozen CH_2Cl_2 for the phbpy complex is shifted to 557 nm for the ph(py)tz complex. Thus, from the emission experiments we conclude a red-shift of the bands when replacing the peripheral pyridine in phbpy through the thiazol in ph(py)tz Pt and Pd complexes.

The left side of Figure 4 shows the TD-DFT calculated UV-vis absorption spectra of the complexes **[M(ph(py)tz)Cl]** and **[M(ph(tbppy)tz)Cl]**. The most intense absorptions are in the range of 210 nm – 350 nm which is in accord with the experimental data (Figure 2 and Table S4). The calculations also verify the experimentally found red shift which occurrs by changing the metal from Pd to Pt. As already discussed, the difference of absorption bands between Pt and Pd is particularly pronounced in the long wavelength range. For the complexes **[M(ph(py)tz)Cl]** broad bands were found at 400 nm for Pd and 430 nm for Pt, respectively. A closer look at the complexes **[M(ph(tbppy)tz)Cl]** reveals a peak at 408 nm for Pd and a peak at around 440 nm for Pt. **[M(ph(py)tz)Cl]** exhibits a small blue shift when compared with **[M(ph(tbppy)tz)Cl]**.

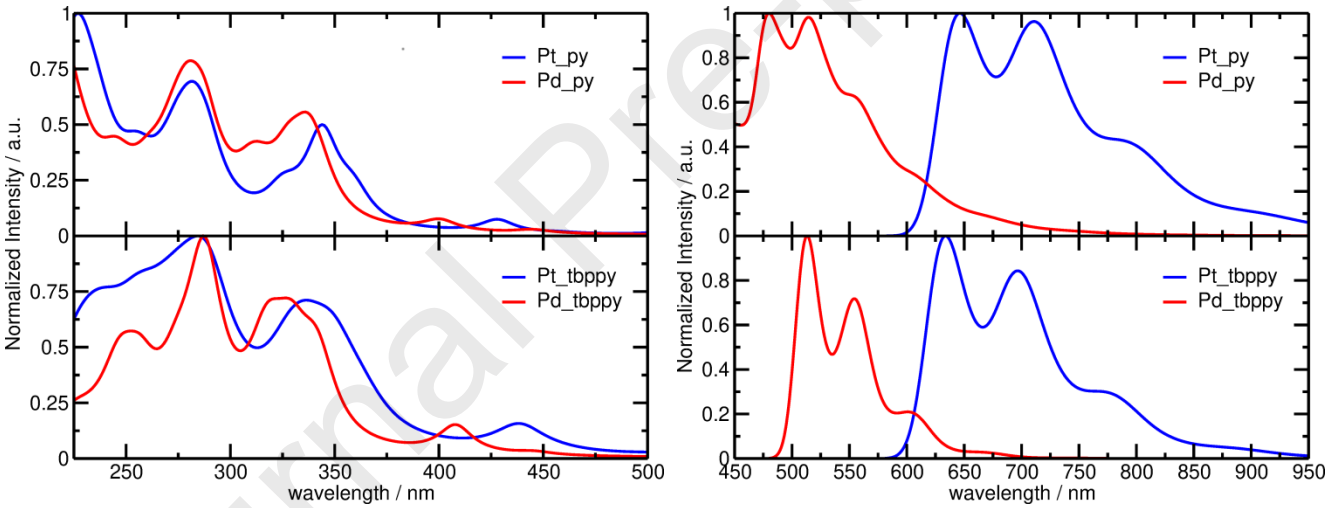

Figure 4. Normalised TD-DFT calculated UV−vis absorption (left) and emission (right) spectra of all four complexes in CH_2Cl_2 at room temperature.

The right side of Figure 4 contains the vibrationally resolved emission spectra at room temperature in CH_2Cl_2. First of all, the experimental result that the change of the ligand substitution pattern for Pt has no significant effect on the emission maxima was confirmed by TD-DFT calculations. Both shape and position are nearly the same for **[Pt(ph(py)tz)Cl]** and **[Pt(ph(tbppy)tz)Cl].** For Pd the shape of the spectrum of **[Pd(ph(py)tz)Cl]** changes in comparison with **[Pd(ph(tbppy)tz)Cl]** while the relative intensity of the main maxima stays similar. The experimentally observed blue shift of the Pd complexes in comparison with the Pt derivatives is clearly confirmed by our TD-DFT calculations.

The most important frontier orbitals of the four complexes at the optimised T_1 geometry are depicted in Figure 5 (left: **[M(ph(py)tz)Cl]** and right: **[M(ph(tbppy)tz)Cl]**). All pictured orbitals have contributions from the ligands and also from the metal centre. The most significant contribution of metal orbitals for all complexes was found at the highest occupied molecular orbital (HOMO). A look at **[M(ph(tbppy)tz)Cl]** shows pronounced delocalisation of the frontier orbitals over the luminophoric ligand, while the contributions on the auxiliary ligand are very small. Furthermore, the HOMO→LUMO excitation is the highest monoelectronic contribution to the T_1 state in all cases. Thus, the T_1 state can be described as a combination of MLCT and IL character of the C^N^N ligand, with some charge transfer character from the phenyl ring to the thiazol moiety. This assignment is consistent with the spin density plots shown in Figure S32.

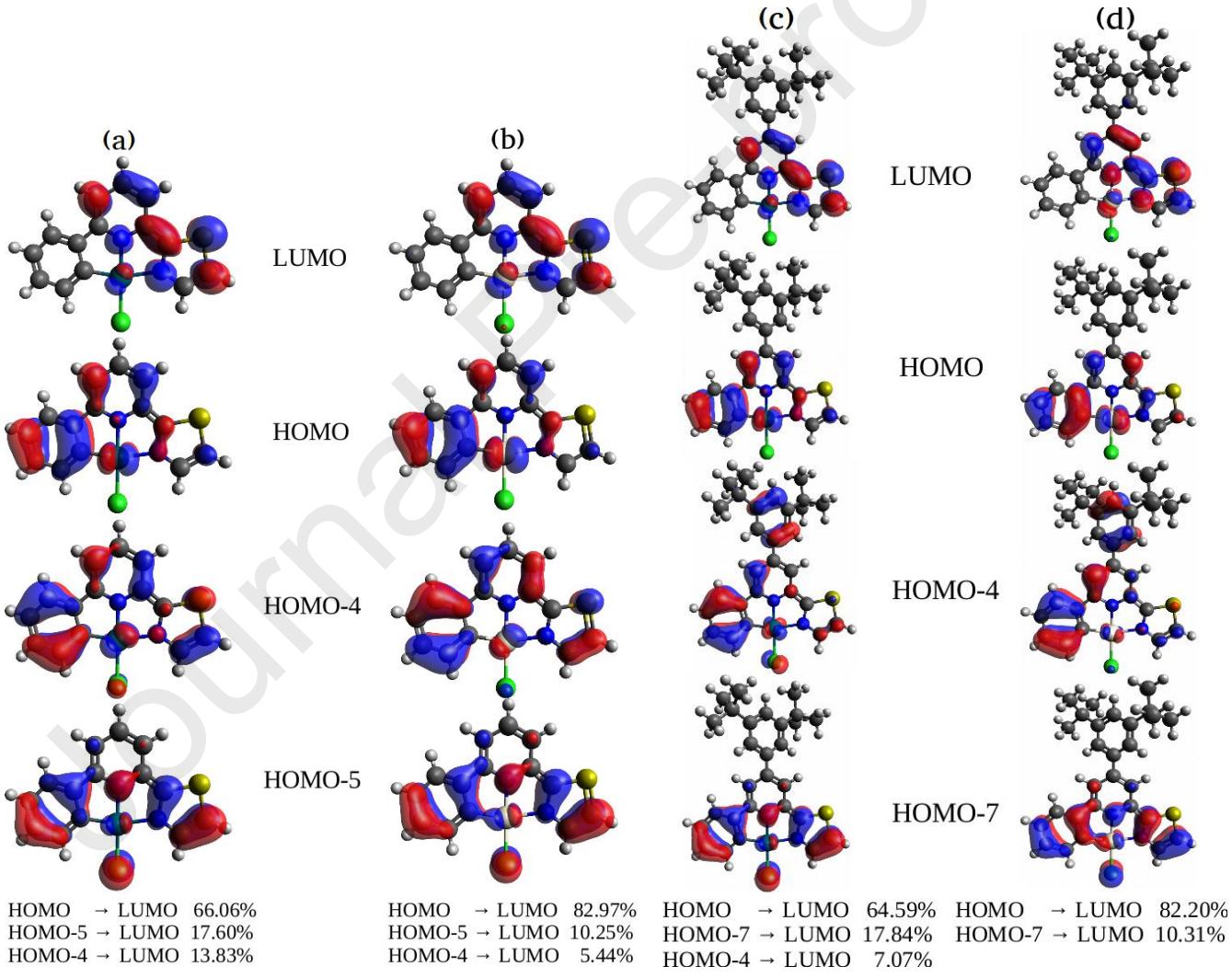

Figure 5. DFT calculated frontier orbitals at the optimised T_1 geometry (a) **[Pd(ph(py)tz)Cl]**, (b) **[Pt(ph(py)tz)Cl]**, (c) **[Pd(ph(tbppy)tz)Cl]** and (d) **[Pt(ph(tbppy)tz)Cl]** together with the contributions (>5%) to the $T_1 \rightarrow S_0$ state obtained by TD-DFT.

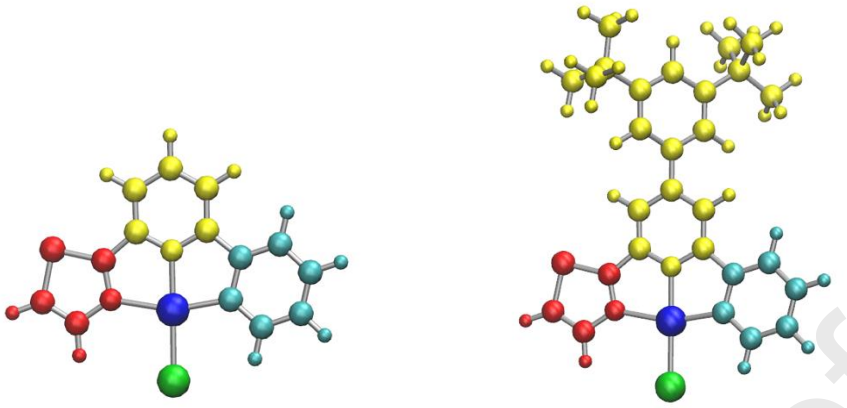

Figure 6. Partitioning of the **[M(ph(py)tz)Cl]** (left) and **[M(ph(tbppy)tz)Cl]** (right) complexes for the numerical analysis of MLCT, LMCT, LC and LLCT excitations shown in Fig. 7.

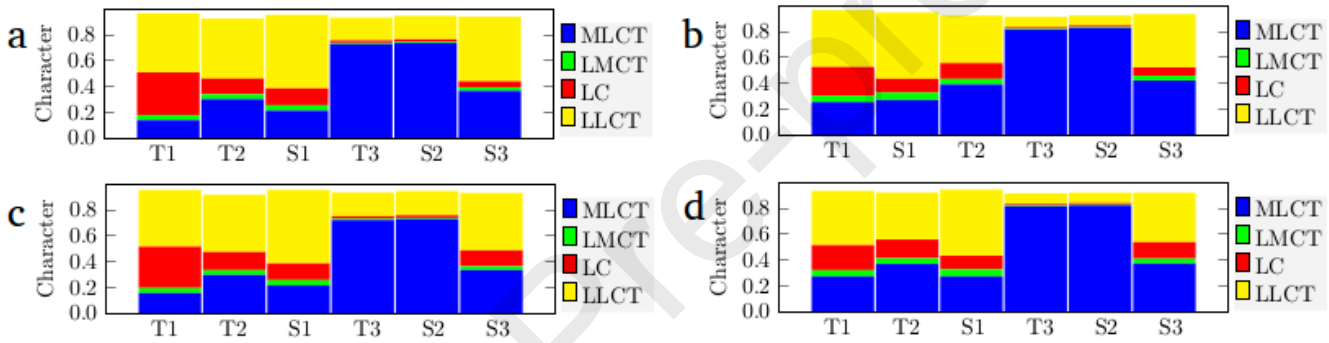

Figure 7. Decomposition into contributions from MLCT, LMCT, LC and LLCT of the first six excited states (in energetical order from left to right) of complexes (a) **[Pd(ph(py)tz)Cl]**, (b) **[Pt(ph(py)tz)Cl]**, (c) **[Pd(ph(tbppy)tz)Cl]** and (d) **[Pt(ph(tbppy)tz)Cl]** computed with the package TheoDORE [69].

With the aid of the package for Theoretical Density, Orbital Relaxation and Exciton analysis (TheoDORE) [69] a more detailed investigation of the excited state character is possible. Figure 7 shows the decomposition into contributions from MLCT, LMCT, LC and LLCT of the first six excited states according to the partitioning defined in Figure 6. It is important to realize that if one treated the entire ligand as a single entity, both LC and LLCT transitions would be described as IL transitions. From Figure 7 it becomes apparent that the Pd complexes have a smaller MLCT character (13-16%) than the Pt derivatives (25-28%). When the **[M(ph(py)tz)Cl]** complex is compared with **[M(ph(tbppy)tz)Cl]**, the latter is the one with the slightly higher MLCT contribution (see Table S7).

3.4 UV-vis spectroelectrochemistry

UV-vis absorption spectroscopy during electrochemical reductions (spectroelectrochemistry, SEC) showed similar patterns for Pd and Pt complexes (Figure 7 and Figures S16-S19) as found for the corresponding

protoligands HC^N^N (Figures S4 and S17), which is in line with a ligand-centred reduction and in agreement with the assignment of the HOMO and LUMO (Section 3.2) and the optical transitions (Section 3.3). Importantly, for all complexes the first reduction occurs reversibly on the (slow) timescale of the SEC experiment, while the second appeared only partly reversible.

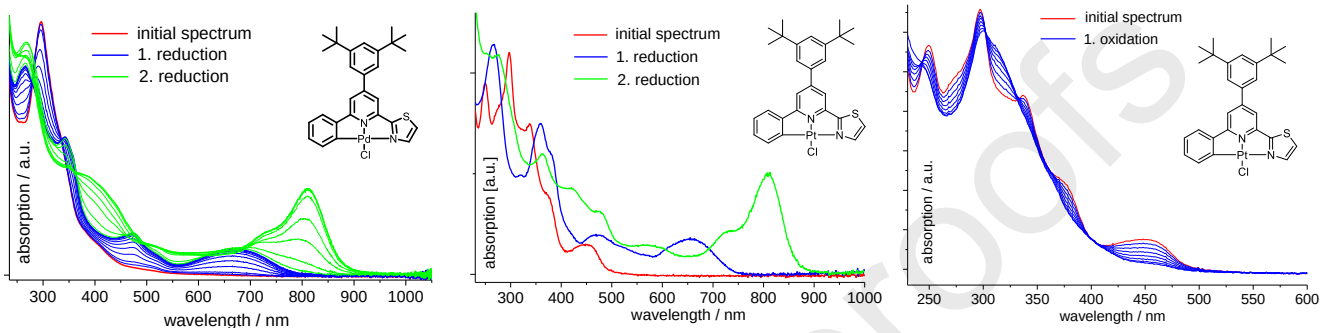

Figure 7. Changes in UV-vis absorption of **[Pd(ph(tbppy)tz)Cl]** (left) and **[Pt(ph(tbppy)tz)Cl]** (middle) during electrochemical reductions and **[Pt(ph(tbppy)tz)Cl]** during oxidations (right) in *n*Bu$_4$NPF$_6$/THF (spectroelectrochemistry, SEC).

During the oxidation of **[Pt(ph(tbppy)tz)Cl]**, the long-wavelength bands at 370 nm and 450 nm disappeared (Figure 7), while the UV bands from 250 to 350 nm were only slightly modified. This is consistent with a metal-centred oxidation and the assignment of the long-wavelength bands of the parent complex at 370 and 450 nm to pronounced MLCT bands and with the TD-DFT calculations (Section 3.3). Oxidation depletes the metal HOMO by one electron, thus decreasing and blue-shifting the MLCT band.

4. Conclusions and outlook

Remarkable differences in the electronic properties were found for four new Pd(II) and Pt(II) complexes [M(C^N^N)Cl] containing tridentate cyclometalating C(phen-ide)^N(py)^N(thiazole) ligands. The variation of the central pyridine (py) to 3,5-(bis-*t*Bu)phenylpyridine (tbppy) for the same central metal (Pd or Pt) resulted in only marginal changes in the ligand-centred reductions, while changing from Pd to Pt led to a small anodic shift of about 50 mV consistent with the largely ligand-centred lowest unoccupied molecular orbitals (LUMO) resulting from DFT calculations. The oxidation potentials are again not very different when varying the ligand but showed a cathodic shift of about 200 mV - 300 mV when going from Pd to Pt. This is consistent with high metal contributions to the highest occupied molecular orbital (HOMO) and was confirmed through DFT. Consquently, the electrochemical HOMO-LUMO gap is decreased from 2.58 eV (Pd) to 2.32 eV (Pt). The long-wavelength absorptions are blue-shifted for the Pd complexes compared with the Pt derivatives consistent with an enlarged HOMO-LUMO gap and thus in line with the electrochemical results. At ambient temperature the

two Pt complexes showed photoluminescence with broad unstructured bands centring at 600 nm. At 77 K in glassy frozen CH_2Cl_2/MeOH all four complexes were luminescent with broad bands showing pronounced vibrational progression. The emission energies of the Pd complexes are markedly blue-shifted compared with the Pt derivatives. TD-DFT calculations were able to confirm this blue-shift for both absorption and emission and showed that this shift goes along with a decreased MLCT contribution and an increased LLCT contribution for the Pd complexes compared with the Pt derivatives. UV-vis absorption spectroelectrochchemistry strongly support the assignments of ligand-centred reductions and a pronounce MLCT contribution to the long-wavelenght absorption bands.

Acknowledgements

The Deutsche Forschungsgemeinschaft [DFG Priority Programme 2102 "Light-controlled Reactivity of Metal Complexes"] DO 768/5-1, STR 1186/6-1, and KL1194/16-1 is acknowledged for funding of this project. We also like to thank Prof. Dr. Mathias Schäfer, Department of Chemistry, University of Cologne for HR-ESI-MS measurements and the Regional Computing Center of the University of Cologne (RRZK) for providing computing time on the DFG-funded High Performance Computing (HPC) system CHEOPS as well as for the support. Simon Schmitz, University of Cologne is acknowledged for the re-refinement of the crystal structures. Furthermore, computer time at the HPC cluster PALMA II at WWU is gratefully acknowledged. CAS would like to acknowledge the Cluster of Excellence Cells in Motion (DFG EXC 1003) for financial support.

Appendix A. Supplementary data

CCDC-2006642 for [Pd(ph(py)tz)Cl] contains the full crystallographic data for this paper. These data can be obtained free of charge from The Cambridge Crystallographic Data Centre via www.ccdc.cam.ac.uk/data_request/cif.

Appendix A. Supplementary data

Tables containing complete crystallographic and structural data were provided together with figures showing the crystal and molecular structure of [Pd(ph(py)tz)Cl]. NMR, UV-vis absorption and cyclic voltammogramms of all four complexes and the two protoligands were provided with data compiled in tables. Emission spectra with time-resolved luminescence decay and DFT calculated LUMO and HOMO compositions were also available.
Supplementary data related to this article can be found at http://dx.doi.org/...

References

[1] J.A.G. Williams, S. Develay, D.L. Rochester, L. Murphy, Optimising the luminescence of platinum(II) complexes and their application in organic light emitting devices (OLEDs), Coord. Chem. Rev. 252 (2008) 2596–2611.

[2] J.A.G. Williams, The coordination chemistry of dipyridylbenzene: N-deficient terpyridine or panacea for brightly luminescent metal complexes?, Chem. Soc. Rev. 38 (2009) 1783–1801.

[3] H. Yersin, A.F. Rausch, R. Czerwieniec, T. Hofbeck, T. Fischer, The triplet state of organo-transition metal compounds. Triplet harvesting and singlet harvesting for efficient OLEDs, Coord. Chem. Rev. 255 (2011) 2622–2652.

[4] V.W.-W. Yam, K.M.-C. Wong, Luminescent metal complexes of d^6, d^8 and d^{10} transition metal centres, Chem. Commun. 47 (2011) 11579–11592.

[5] S. Archer, J.A. Weinstein, Charge-separated excited states in platinum(II) chromophores: Photophysics, formation, stabilization and utilization in solar energy conversion, Coord. Chem. Rev. 256 (2012) 2530–2561.

[6] P.K. Chow, C. Ma, W.-P. To, G.S.M. Tong, S.-L. Lai, S.C.F. Kui, W.-M. Kwok, C.-M. Che, Strongly Phosphorescent Palladium(II) Complexes of Tetradentate Ligands with Mixed Oxygen, Carbon, and Nitrogen Donor Atoms: Photophysics, Photochemistry, and Applications, Angew. Chem., Int. Ed. 52 (2013) 11775 –11779.

[7] J. Zhao, W. Wu, J. Sun, S. Guo, Triplet photosensitizers: from molecular design to applications, Chem. Soc. Rev. 42 (2013) 5323–5351.

[8] K. Li, G.S.M. Tong, Q. Wan, G. Cheng, W.-Y. Tong, W.-H. Ang, W.-L. Kwong, C.-M. Che, Highly phosphorescent platinum(II) emitters: photophysics, materials and biological application, Chem. Sci. 7 (2016) 1653–1673.

[9] P.-K. Chow, G. Cheng, G.S.M. Tong, C. Ma, W.-M. Kwok, W.-H. Ang, C.Y.-S. Chung, C. Yang, F. Wang, C.-M. Che, Highly luminescent palladium(II) complexes with sub-millisecond blue to green phosphorescent excited states. Photocatalysis and highly efficient PSF-OLEDs, Chem. Sci. 7 (2016) 6083–6098.

[10] M. Krause, D. Kourkoulos, D. González-Abradelo, K. Meerholz, C. A. Strassert, A. Klein, Luminescent Pt^{II} Complexes of Tridentate Cyclometalating 2,5-Bis(aryl)-pyridine Ligands, Eur. J. Inorg. Chem. 2017 (2017) 5215–5223.

[11] T. Fleetham, G. Li, J. Li, Phosphorescent Pt(II) and Pd(II) Complexes for Efficient, High-Color-Quality, and Stable OLEDs, Adv. Mater. 29 (2017) 1601861 (1–16).

[12] Y. Zhang, Y. Wang, J. Song, J. Qu, B. Li, W. Zhu, W-Y. Wong, Near-Infrared Emitting Materials via Harvesting Triplet Excitons: Molecular Design, Properties, and Application in Organic Light Emitting Diodes, Adv. Optical Mater. 6 (2018) 1800466 (1–19).

[13] C. Zou, J. Lin, S. Suo, M. Xie, X. Chang, W. Lu, Palladium(II) N-heterocyclic allenylidene complexes with extended intercationic Pd···Pd interactions and MMLCT phosphorescence, Chem. Commun. 54 (2018) 5319–5322.

[14] Q. Wan, W.-P. To, C. Yang, C.-M. Che, The Metal–Metal-to-Ligand Charge Transfer Excited State and Supramolecular Polymerization of Luminescent Pincer Pd^{II}–Isocyanide Complexes, Angew. Chem., Int. Ed. 57 (2018) 3089–3093.

[15] L. Liu, X. Wang, F. Hussain, C. Zeng, B. Wang, Z. Li, I. Kozin, S. Wang, Multiresponsive Tetradentate Phosphorescent Metal Complexes as Highly Sensitive and Robust Luminescent Oxygen Sensors: Pd(II) Versus Pt(II) and 1,2,3-Triazolyl Versus 1,2,4-Triazolyl, ACS Appl. Mater. Interfaces 11 (2019) 12666−12674

[16] Y. Yao, C.-L. Hou, Z.-S. Yang, G. Ran, L. Kang, C. Li, W. Zhang, J. Zhang, J.-L. Zhang, Unusual near infrared (NIR) fluorescent palladium(II) macrocyclic complexes containing M–C bonds with bioimaging capability, Chem. Sci. 10 (2019) 10170–10178.

[17] X. Wang, S. Wang, Phosphorescent Pt(II) Emitters for OLEDs: From Triarylboron-Functionalized Bidentate Complexes to Compounds with Macrocyclic Chelating Ligands, Chem. Rec. 19 (2019) 1–18.

[18] G. Cheng, Y. Kwak, W.-P. To, T.-L. Lam, G.S.M. Tong, M.-K. Sit, S. Gong, B. Choi, W.i. Choi, C. Yang, C.-M. Che, High-Efficiency Solution-Processed Organic Light-Emitting Diodes with Tetradentate Platinum(II) Emitters, ACS Appl. Mater. Interfaces 11 (2019) 45161−45170.

[19] I.O. Koshevoy, M. Krause, A. Klein, Non-Covalent Intramolecular Interactions through Ligand-Design Promoting Efficient Luminescence from Transition Metal Complexes, Coord. Chem. Rev. 405 (2020) 213094 (1–17).

[20] V.W.-W. Yam, A.S.-Y. Law, Luminescent d^8 metal complexes of platinum(II) and gold(III): From photophysics to photofunctional materials and probes, Coord. Chem. Rev. 414 (2020) 213–298.

[21] J. Föller, D.H. Friese, S. Riese, J.M. Kaminski, S. Metz, D. Schmidt, F. Würthner, C. Lambert, C.M. Marian, On the photophysical properties of Ir^{III}, Pt^{II}, and Pd^{II} (phenylpyrazole) (phenyldipyrrin) complexes, Phys. Chem. Chem. Phys. 22 (2020) 3217–3233.

[22] A. Heil, C.M. Marian, Structure−Emission Property Relationships in Cyclometalated Pt(II) β-Diketonate Complexes, Inorg. Chem. 58 (2019) 6123−6136.

[23] Y. Luo, Z. Chen, J. Hu, Z. Xu, Q. Meng, D. Tang, Small substituent groups as geometric controllers for tridentate platinum(II) complexes to effectively suppress non-radiative decay processes, Phys. Chem. Chem. Phys. 21 (2019) 2764–2770.

[24] W. Cai, H. Zhang, X. Yan, A. Zhao, R. He, M. Li, Q. Meng, W. Shen, What accounts for the color purity of tetradentate Pt complexes? A computational analysis, Phys. Chem. Chem. Phys. 21 (2019) 8073–8080.

[25] Y.-T. Liu, Y.-R. Li, X. Wang, F.-Q. Bai, Theoretical investigation of N^C^N-coordinated Pt(II) and Pd(II) complexes for long-lived two-photon photodynamic therapy, Dyes Pigm. 142 (2017) 55–61.

[26] T.-T. Feng, F.-Q. Bai, L.-M. Xie, Y. Tang, H.-X. Zhang, Theoretical study and design of highly efficient platinum(II) complexes bearing tetradentate ligands for OLED, RSC Adv. 6 (2016) 11648–11656.

[27] J. Sanning, L. Stegemann, P.R. Ewen, C. Schwermann, C.G. Daniliuc, D. Zhang, N. Lin, L. Duan, D. Wegner, N.L. Doltsinis, C.A. Strassert, Colour-tunable asymmetric cyclometalated Pt(II) complexes and STM-assisted stability assessment of ancillary ligands for OLEDs, J. Mater. Chem. C 4 (2016) 2560–2565.

[28] L. Wang, J. Wen, H. He, J. Zhang, The reasons for ligand-dependent quantum yields and spectroscopic properties of platinum(II) complexes based on tetradentate O^N^C^N ligands: a DFT and TD-DFT study, Dalton Trans. 43 (2014) 2849–2858.

[29] S.C.F. Kui, F.-F. Hung, S.-L. Lai, M.-Y. Yuen, C.-C. Kwok, K.-H. Low, S.S.-Y. Chui, C.-M. Che, Luminescent Organoplatinum(II) Complexes with Functionalized Cyclometalated C^N^C Ligands: Structures, Photophysical Properties, and Material Applications, Chem.–Eur. J. 18 (2012) 96–109.

[30] L. Wang, Y. Zhang, J. Li, H. He, J. Zhang, Influence of primary and auxiliary ligand on spectroscopic properties and luminescent efficiency of organoplatinum(II) complexes bearing functionalized cyclometalated C^N^C ligands, Dalton Trans. 43 (2014) 14029–14038.

[31] G. S.-M. Tong, C.-M. Che, Emissive or Nonemissive? A Theoretical Analysis of the Phosphorescence Efficiencies of Cyclometalated Platinum(II) Complexes, Chem.–Eur. J. 15 (2009) 7225–7237.

[32] Z. Wu, T. Xie, Y. Luo, W. Zhuo, J. Gu, X. Yan, X. Sun, K. Zuo, X. Liu, Y. Gan, L. Liang, G. He, W. Liu, X. Gou, D. Tang, H. Shi, J. Hu, Theoretical insight into the photodeactivation pathway of the tetradentate Pt (II) complex with different inductive substituents, Appl. Organometal. Chem. 33 (2019) e4879 (1–12).

[33] S. Poirier, H. Lynn, C. Reber, Variation of M···H–C Interactions in Square-Planar Complexes of Nickel(II), Palladium(II), and Platinum(II) Probed by Luminescence Spectroscopy and X‑ray Diffraction at Variable Pressure, Inorg. Chem. 57 (2018) 7713−7723.

[34] S.S. Attar, F. Artizzu, L. Marchik, D. Espa, L. Pilia, M.F. Casula, A. Serpe, M. Pizzotti, A. Orbelli-Biroli, P. Deplano, Uncommon Optical Properties and Silver-Responsive Turn-Off/On Luminescence in a Pt^{II} Heteroleptic Dithiolene Complex, Chem.–Eur. J. 24 (2018) 10503–10512.

[35] A.M. Potocny, A.J. Pistner, G.P.A. Yap, J. Rosenthal, Electrochemical, Spectroscopic, and $^1O_2$ Sensitization Characteristics of Synthetically Accessible Linear Tetrapyrrole Complexes of Palladium and Platinum, Inorg. Chem. 56 (2017) 12703−12711.

[36] P. Kar, M. Yoshida, A. Kobayashi, L. Routaboul, P. Braunstein, M. Kato, Colour tuning by the stepwise synthesis of mononuclear and homo- and hetero-dinuclear platinum(II) complexes using a zwitterionic quinonoid ligand, Dalton Trans. 45 (2016) 14080–14088.

[37] E.A. Katlenok, K.P. Balashev, Optical and Electrochemical Properties of Cyclometalated Pd(II) and Pt(II) Complexes with a Metal–Metal Chemical Bond, Opt. Spectrosc. 116 (2014) 100–104.

[38] E.A. Katlenok, K.P. Balashev, Optical, Spectroscopic, and Electrochemical Properties of Cyclometalated Complexes of Platinum Metals Based on 2-Tolylpyridine and Benzo[h]quinoline in Ethylenediamine, Opt. Spectrosc. 115 (2013) 518–522.

[39] M.M. Nevdakh, M.V. Puzyk, Specific Features of Spectra of Cyclometalated Pt(II) and Pd(II) Complexes in Polyvinyl Alcohol, Opt. Spectrosc. 96 (2004) 816–818.

[40] M.V. Puzyk, M.A. Ivanov, K.P. Balashev, Effect of the Nature of Heterocyclic Ligands on Spectral and Luminescent Properties of Pt(II) and Pd(II) Complexes, Opt. Spectrosc. 95 (2003) 581–584.

[41] D. Song, Q. Wu, A. Hook, I. Kozin, S. Wang, Syntheses and Structures of New Luminescent Cyclometalated Palladium(II) and Platinum(II) Complexes: M(Bab)Cl, M(Br-Bab)Cl (M = Pd(II), Pt(II)), and $Pd_3Cl_4(Tab)_2$ (Bab = 1,3-bis(7-azaindolyl)phenyl, Br-Bab = 1-Bromo-3,5-bis(7-azaindolyl)phenyl, Tab = 1,3,5-tris(7-azaindolyl)phenyl), Organometallics 20 (2001) 4683–4689.

[42] S.-W. Lai, T.-C. Cheung, M. C. W. Chan, K.-K. Cheung, S.-M. Peng, C.-M. Che, Luminescent Mononuclear and Binuclear Cyclometalated Palladium(II) Complexes of 6-Phenyl-2,2′-bipyridines: Spectroscopic and Structural Comparisons with Platinum(II) Analogues, Inorg. Chem. 39 (2000) 255–262.

[43] P. Jolliet, M. Gianini, A. von Zelewsky, G. Bernardinelli, H. Stoeckli-Evans, Cyclometalated Complexes of Palladium(II) and Platinum(II): cis-Configured Homoleptic and Heteroleptic Compounds with Aromatic C^N Ligands, Inorg. Chem. 35 (1996) 4883–4888.

[44] P.P. Phadnis, V.K. Jain, T. Schurr, A. Klein, F. Lissner, Th. Schleid, W. Kaim, Synthesis, spectroscopy, structure and photophysical properties of dinaphthylmethylarsine complexes of palladium(II) and platinum(II), Inorg. Chim. Acta 358 (2005) 2609–2617.

[45] S. Dey, L.B. Kumbhare, V.K. Jain, A. Klein, T. Schurr, W. Kaim, F. Belaj, Structural Varieties in 1-Dimethylaminopropyl-2-chalcogenolate and 2-Dimethylaminopropyl-1-chalcogenolate (S, Se, Te) Complexes of Palladium(II) and Platinum(II): Synthesis, Spectroscopy and Structures, Eur. J. Inorg. Chem. 2004 (2004) 4510–4520.

[46] P.P. Phadnis, V.K. Jain, A. Klein, M. Weber, W. Kaim, Configurational selectivity in benzyldimethylarsine complexes of palladium(II) and platinum(II): Synthesis, spectroscopy and structures, Inorg. Chim. Acta 346 (2003) 119–128.

[47] F. Neve, A. Crispini, S. Campagna, Anisometric Cyclometalated Palladium(II) and Platinum(II) Complexes. Structural and Photophysical Studies, Inorg. Chem. 36 (1997) 6150–6156.

[48] W. Kaim. J. Fiedler, J. Spectroelectrochemistry: the best of two worlds, Chem. Soc. Rev. 38 (2009) 3373–3382.

[49] W. Kaim, A. Klein, Spectroelectrochemistry, Cambridge, UK, RSC Publishing, 2008.

[50] M.C. Burla, R. Caliandro, B. Carrozzini, G.L. Cascarano, C. Cuocci, C. Giacovazzo, M. Mallamo, A. Mazzone, G. Polidori, G. Crystal structure determination and refinement via SIR2014, J. Appl. Crystallogr. 48 (2015) 306–309.

[51] G.M. Sheldrick, SHELXL 2016. A short history of *SHELX*, Acta Crystallogr., Sect. A: Found. Crystallogr. 64 (2008) 112–122.

[52] M.J. Frisch, G.W. Trucks, H.B. Schlegel, G.E. Scuseria, M.A. Robb, J.R. Cheeseman, G. Scalmani, V. Barone, B. Mennucci, G.A. Petersson, et al. Gaussian 09, Revision D.01. 2009; Gaussian Inc. Wallingford CT 2009.

[53] T. Yanai, D.P. Tew, N.C. Handy, A new hybrid exchange–correlation functional using the Coulomb-attenuating method (CAM-B3LYP), Chem. Phys. Lett. 293 (2004) 51–57.

[54] S. Grimme, S. Ehrlich, L. Goerigk, Effect of the damping function in dispersion corrected density functional theory, J. Comp. Chem. 32 (2011) 1456–1465,

[55] D. Andrae, U. Häußermann, M. Dolg, H. Stoll, H. Preuß, Energy-adjusted ab initio pseudopotentials for the second and third row transition elements, Theor. Chim. Acta 77 (1990) 123–141.

[56] T.H. Dunning, P.J. Hay, in H.F. Schaefer III (ed.), Modern Theoretical Chemistry; Plenum, New York, 1976; Vol. 3, pp. 1-28.

[57] V. Barone, J. Bloino, M. Biczysko, Vibrationally-resolved electronic spectra in GAUSSIAN 09, GAUSSIAN 09 Revision A.02 (2009) 1–20.

[58] V. Barone, J. Bloino, M. Biczysko, F. Santoro, Fully Integrated Approach to Compute Vibrationally Resolved Optical Spectra: From Small Molecules to Macrosystems, J. Chem. Theory Comput. 5 (2009) 540–554.

[59] J. Tomasi, B. Mennucci, R. Cammi, Quantum Mechanical Continuum Solvation Models, Chem. Rev. 105 (2005) 2999–3094.

[60] A. K. Rappé, C. J. Casewit, K. S. Colwell, W. A. Goddard III, W. M. Skiff, UFF, a Full Periodic Table Force Field for Molecular Mechanics and Molecular Dynamics Simulations, J. Am. Chem. Soc. 114 (1992) 10024–10035.

[61] C. Adamo, V. Barone, Toward reliable density functional methods without adjustable parameters: The PBE0 model, J. Chem. Phys. (1999) 6158–6170.

[62] G.-J. Zhang, X. Gan, Q.-Q. Xu, Y. Chen, X.-J. Zhao, B. Qin, X.-J Lv, S.-W. Lai, W.-F. Fu, C.-M. Che, Photophysical and electrochemical properties of platinum(II) complexes bearing a chromophore–acceptor dyad and their photocatalytic hydrogen Evolution, Dalton Trans. 41 (2012) 8421–8429.

[63] M.-Y. Yuen, S.C.F. Kui, K.-H. Low, C.-C. Kwok, S.S.-Y. Chui, C.-W. Ma, N. Zhu, C.-M. Che Synthesis, Photophysical and Electrophosphorescent Properties of Fluorene-Based Platinum(II) Complexes, Chem.–Eur. J. 16 (2010) 14131–14141.

[64] M. Zvirzdinaite, S. Garbe, N. Arefyeva, M. Krause, R. von der Stück, A. Klein, Palladium(II) Complexes of Ambidentate and Potentially Cyclometalating 5-Aryl-3-(2′-pyridyl)-1,2,4-triazine Ligands, Eur. J. Inorg. Chem. 2017 (2017) 2011–2022.

[65] V. Lingen, A. Lüning, C. Strauß, I. Pantenburg, G.B. Deacon, A. Klein, G. Meyer, Palladium Complexes with the SC_6F_4H-4 Ligand – Synthesis, Spectroscopy, and Structures, Eur. J. Inorg. Chem. 2013 (2013) 4450–4458.

[66] K. Butsch, R. Gust, A. Klein, I. Ott, M. Romanski, Tuning the electronic properties of dppz-ligands and their palladium(II) Complexes, Dalton Trans. 39 (2010) 4331–4340.

[67] A. Klein, M. Niemeyer, Synthesis, Coordination, and Spectroscopic Properties of 2,2'-Bipyridyldimesitylpalladium(II) and 6-Mesityl-2,2'-bipyridyldimesitylpalladium(II), Z. Anorg. Allg. Chem. 626 (2000) 1191–1195.

[67] T.-C. Cheung, K.-K. Cheung, S.-M. Peng, C.-M. Che, Photoluminescent cyclometallated diplatinum(II,II) complexes: photophysical properties and crystal structures of $[PtL(PPh_3)]ClO_4$ and $[Pt_2L_2(\mu\text{-dppm})][ClO_4]$ (HL = 6-phenyl-2,2'-bipyridine, dppm = $Ph_2PCH_2PPh_2$), J. Chem. Soc., Dalton Trans. (1996) 1645–1651.

[68] F. Neve, A. Crispini, C. Di Pietro, S. Campagna, Light-Emitting Cyclopalladated Complexes of 6-Phenyl-2,2′-bipyridines with Hydrogen-Bonding Functionality, Organometallics 21 (2002) 3511–3518.

[69] F. Plasser, TheoDORE: A Toolbox for a Detailed and Automated Analysis of Electronic Excited State Computations, J. Chem. Phys. 152 (2020) 084108 (1–14).

Highlights:

- Cyclometalated Pd(II) and Pt(II) complexes with tridentate C^N^N ligands (C = phenyl, N = pyridyl; N = thiazol) were studied for their electronic properties in comparison
- Pt(II) complexes showed orange photoluminescence at 298 K, while for Pd(II) emission is observed at 77 K. At 77 K, Pt(II) and Pd(II) complexes show similar quantum yields around 20%.
- Quantum chemical TD-DFT allowed to trace these differences to different contributions of the three ligand parts and higher ^{3}IL character for Pd(II) compared with higher ^{3}MLCT character for Pt(II).

Maren Krause: Investigation, Data curation, Visualisation. **Rene von der Stück**: Investigation, Data curation, Visualisation. **Dana Brünkink:** Investigation, Data curation, Visualisation. **Stefan Buss:** Investigation, Data curation, Visualisation. **Nikos L. Doltsinis:** Methodology, Validation, Writing- Original draft preparation, Writing - Review & Editing, Supervision, Project Administration, Funding acquisition. **Cristian A. Strassert**: Methodology, Validation, Formal analysis, Writing- Original draft preparation, Writing - Review & Editing, Supervision, Project Administration, Funding acquisition. **Axel Klein:** Methodology, Validation, Visualisation, Writing- Original draft preparation, Writing - Review & Editing, Supervision, Project Administration, Funding acquisition.